Supplementary Information

Gold-bridged $LaCo_{1-x}Au_xO_3$ perovskite nanocomposite for synergically enhanced electrochemical hydrogen storage

Maryam Ostadebrahim,[a] Mohammad Qorbani,*[bc] Amr Sabbah,*[def] Ying-Ren Lai,*[de] Mohammad Soleimani,[g] Michitoshi Hayashi,[deh] Li-Chyong Chen,[dei] Kuei-Hsien Chen,[dj] and Omran Moradlou*[aj]

[a]Department of Analytical Chemistry, Faculty of Chemistry, Alzahra University, Tehran 19938-93973, Iran.

Email: moradlou@as.edu.tw; moradlou@alzahra.ac.ir

[b]Undergraduate Program of Electro-Optical Engineering, National Taiwan Normal University, Taipei 11677, Taiwan.

Email: qorbani@ntnu.edu.tw

[c]Institute of Electro-Optical Engineering, National Taiwan Normal University, Taipei 11677, Taiwan

[d]Center for Condensed Matter Sciences, National Taiwan University, Taipei 10617, Taiwan.

Email: amrsabbah@ntu.edu.tw; yingrenlai@ntu.edu.tw

[e]Center of Atomic Initiative for New Materials, National Taiwan University, Taipei 10617, Taiwan.

[f]Tabbin Institute for Metallurgical Studies, Tabbin, Helwan 109, Cairo 11421, Egypt.

[g]Shimi Gen Pharmed, Saveh Industrial City, Saveh 39141-71984, Iran

[h]National Center for Theoretical Sciences, Taipei 10617, Taiwan.

[i]Department of Physics, National Taiwan University, Taipei 10617, Taiwan.

[j]Institute of Atomic and Molecular Sciences, Academia Sinica, Taipei 10617, Taiwan.

Supplementary Figures

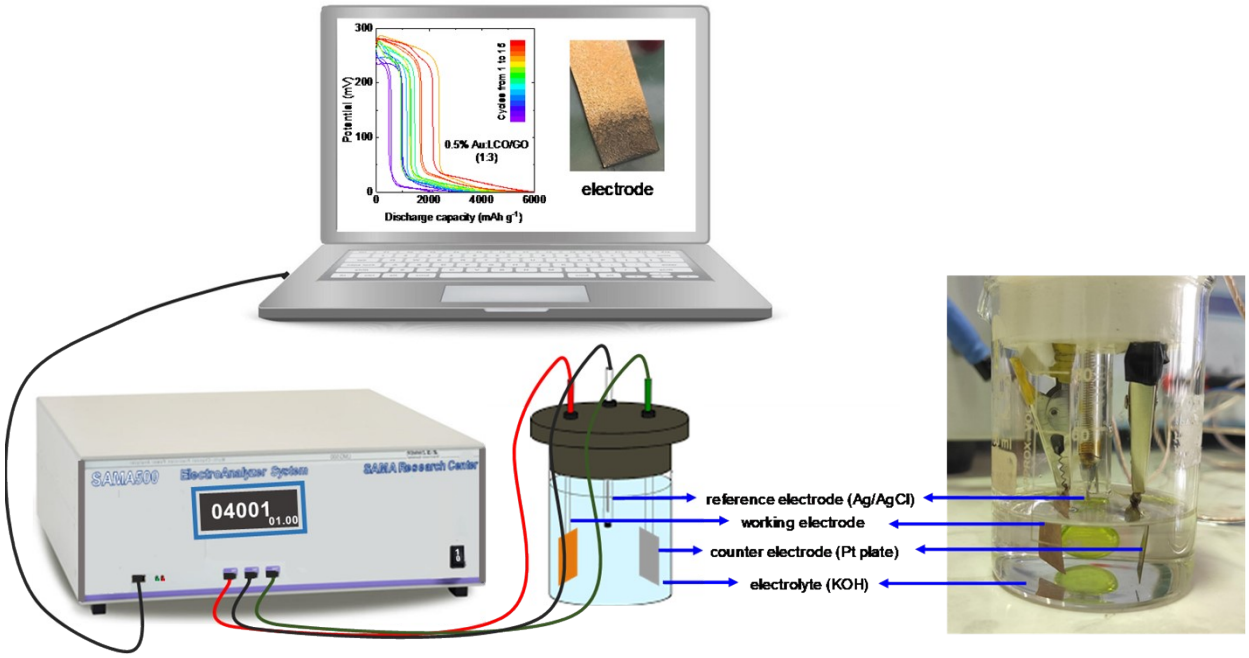

Fig. S1 Hydrogen storage experimental setup. Hydrogen storage capacity of the samples was measured by GCD tests at a constant current of 1 mA (or 3.3 A g^{-1}) using a SAMA 500 Electro-Analyzer system.

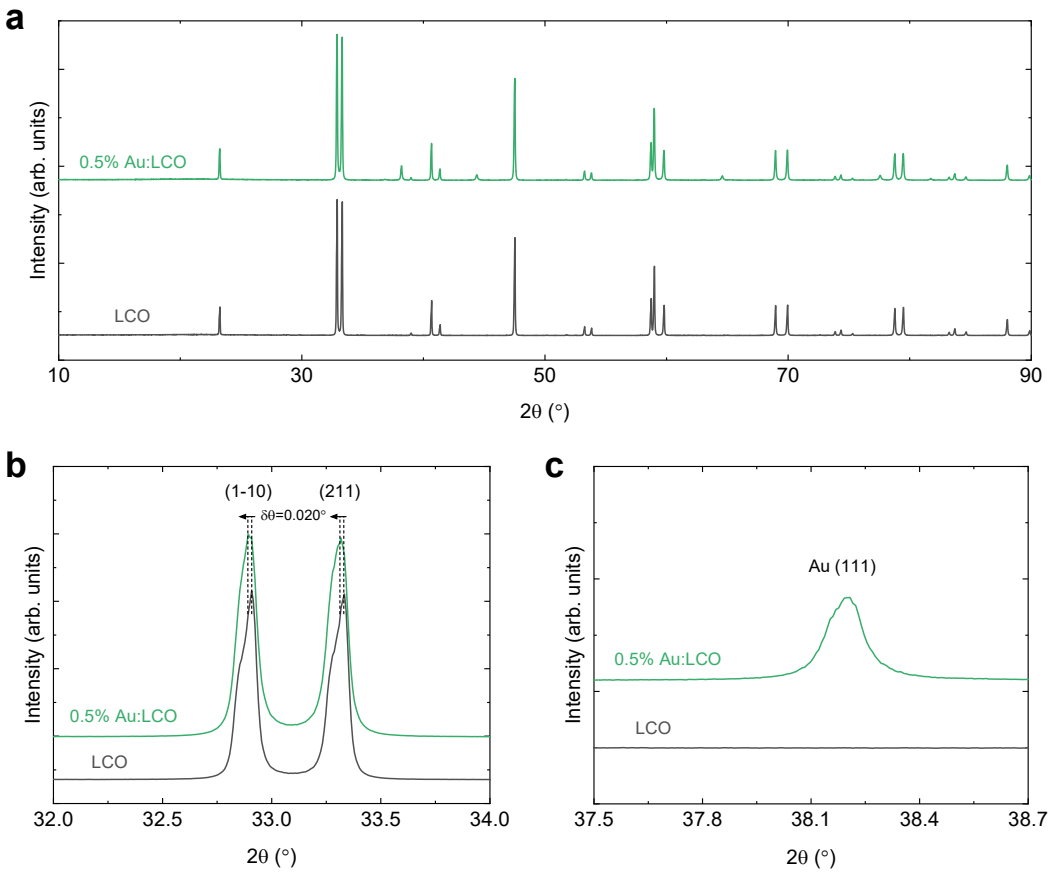

Fig. S2 (**a**) Synchrotron XRD patterns of LCO and 0.5% Au:LCO. (**b**–**c**) XRD patterns corresponding to the (1-10) and (211) LCO or 0.5% Au:LCO and Au (111) crystalline planes, respectively. The observed bifurcation of the (1-10) and (211) peaks are the characteristic peak of the rhombohedral structure might be due to the distortion in the crystal structure.[1, 2]

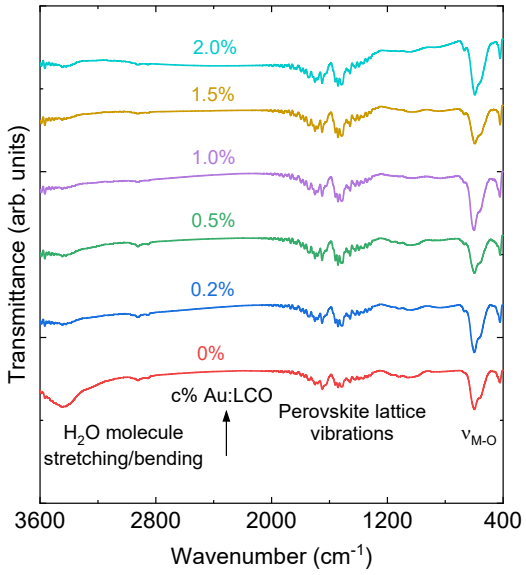

Fig. S3 FTIR spectra of c% Au:LCO where c = 0 to 2.0 at%.

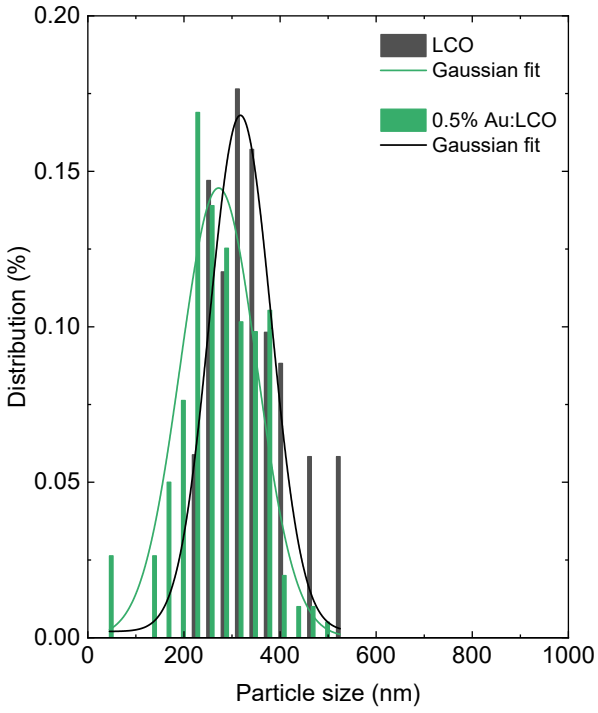

Fig. S4 Particle size distributions of the LCO and 0.5% Au:LCO measured from their FE-SEM images with a scale of 500 nm.

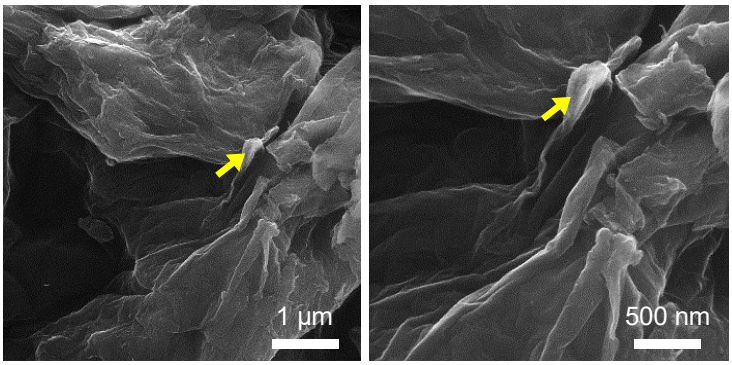

Fig. S5 FE-SEM images of GO nanosheets at different magnifications. Yellow arrows guide the eyes to the zoomed-in region in each image.

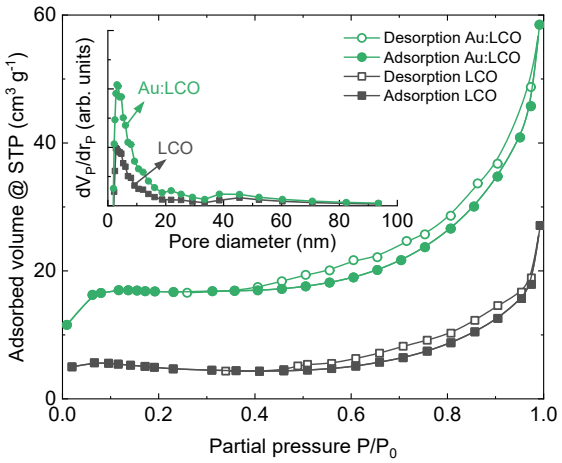

Fig. S6 BET N_2 adsorption/desorption curves of LCO and 0.5% Au:LCO. Inset shows the pore size distribution curves.

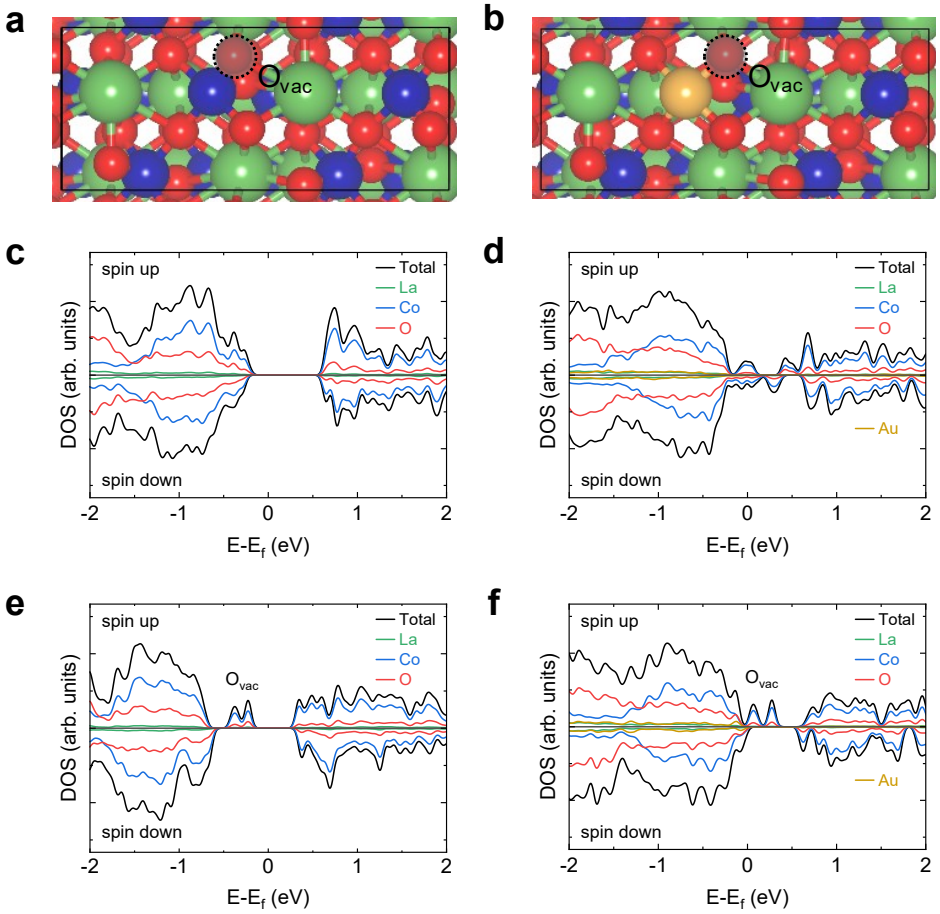

Fig. S7 (a–d) The atomic configurations of LCO and Au:LCO with O_{vac} and **(c–f)** Calculated DOS of LCO, Au:LCO, LCO with O_{vac}, Au:LCO with O_{vac}, respectively. Green, blue, red, and orange spheres stand for La, Co, O, and Au atoms, respectively.

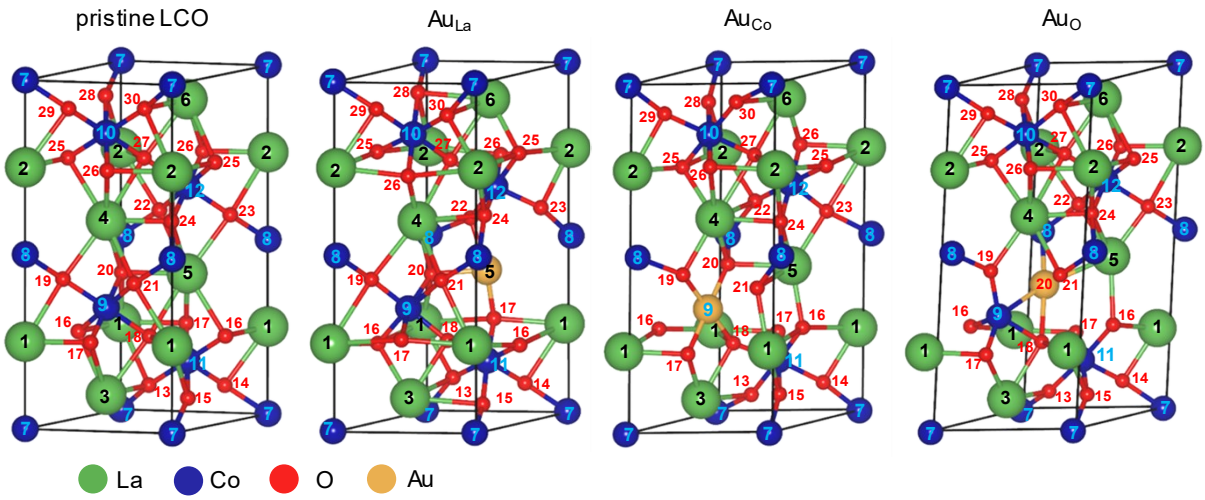

Fig. S8 DFT-calculated relaxed configurations with corresponding atom numbers. Green, blue, red, and orange spheres stand for La, Co, O, and Au atoms, respectively.

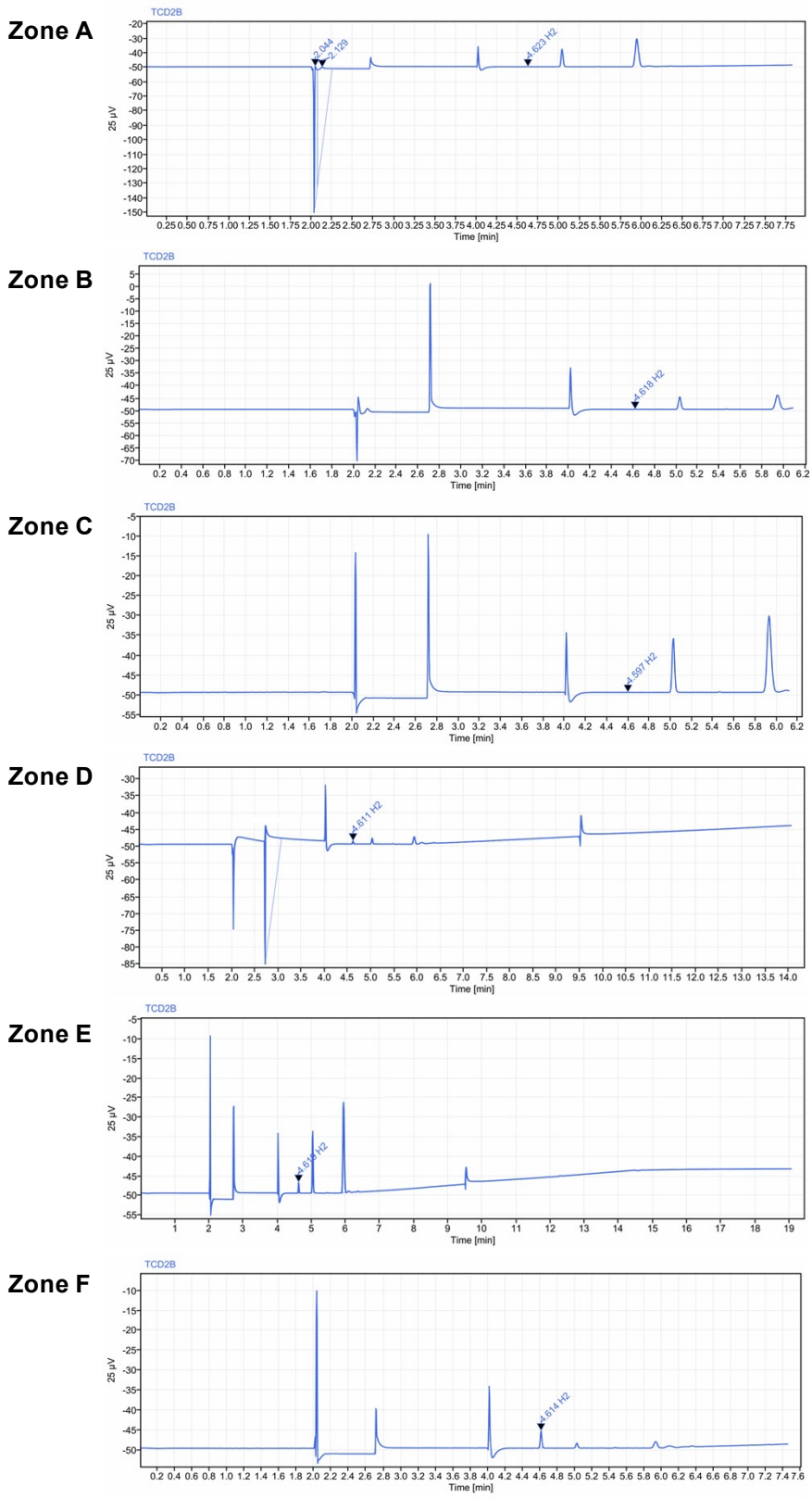

Fig. S9 The chromatograms of the zones illustrated in Fig. 6b.

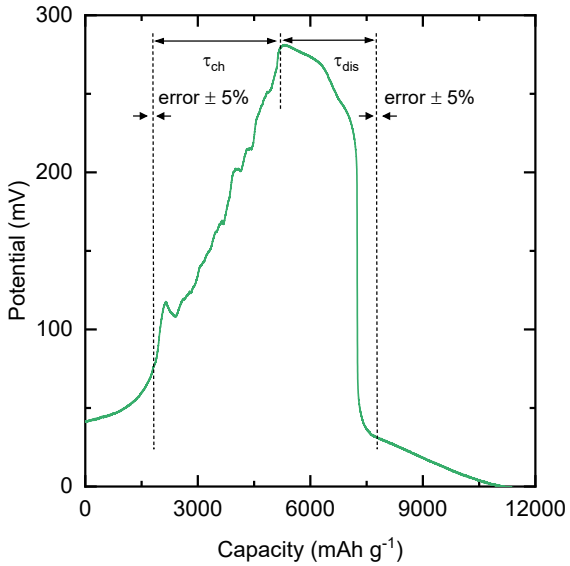

Fig. S10 Charge and Discharge capacity profile 0.5% Au:LCO/GO (1:3) under 1 mA current for 15th cycle. Coulombic efficiency is calculated by the $\frac{\tau_{dis}}{\tau_{ch}}$ ratio. We note that the associated uncertainty is approximately 10%, which arises from the intrinsic challenge of precisely determining the onset potentials.

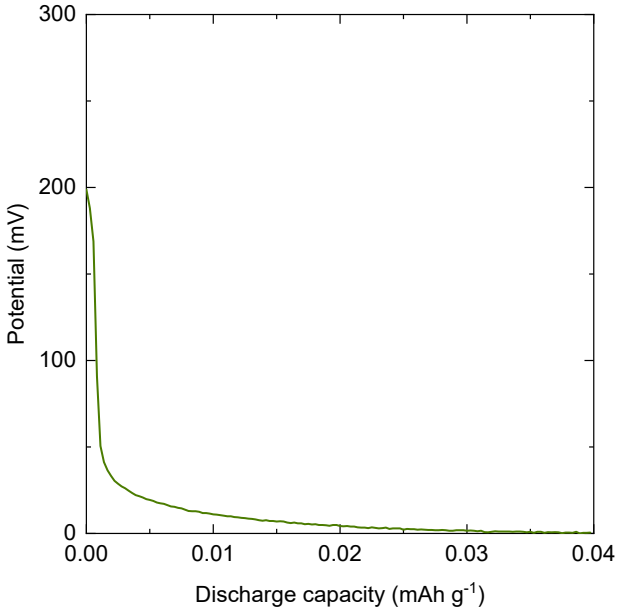

Fig. S11 Discharge capacity profile of copper electrode under 1 mA current.

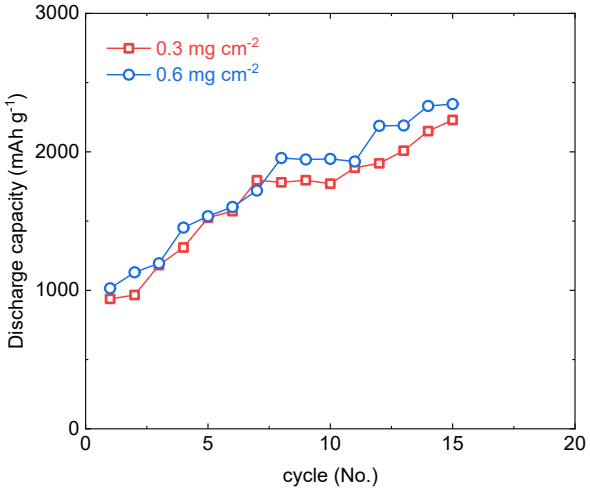

Fig. S12 The impact of loading mass on the capacity of 0.5% Au:LCO/GO (1:3).

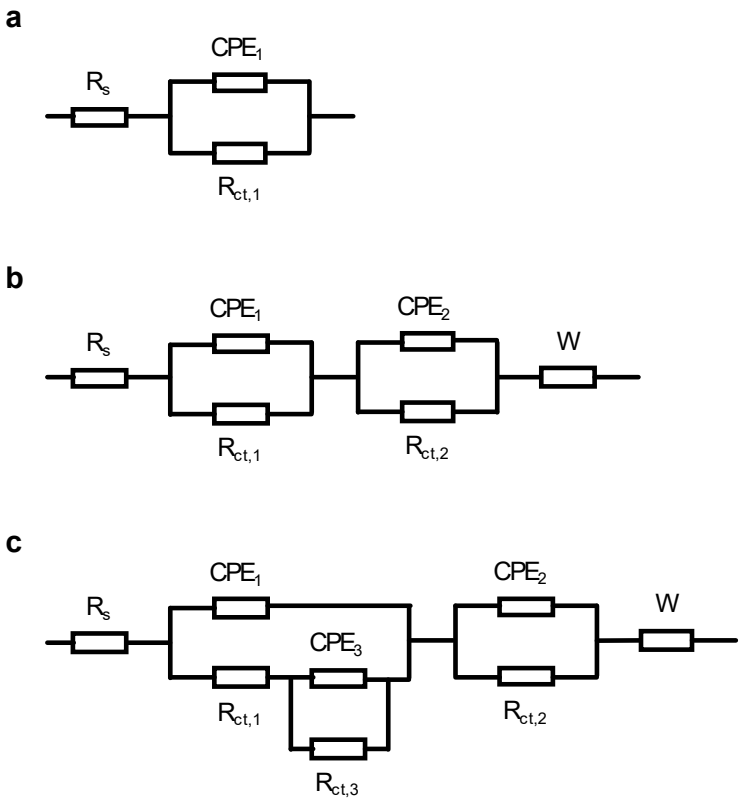

Fig. S13 Equivalent circuits used to fit the EIS data: **(a)** GO ($R_s + [R_{ct,1}||CPE_1]$), **(b)** LCO or 0.5% Au:LCO ($R_s + [R_{ct,1}||CPE_1] + [R_{ct,2}||CPE_2]$), and **(c)** 0.5% Au:LCO/GO (1:3) ($R_s + [R_{ct,1}||CPE_1]||[R_{ct,3}||CPE_3] + [R_{ct,2}||CPE_2]$).

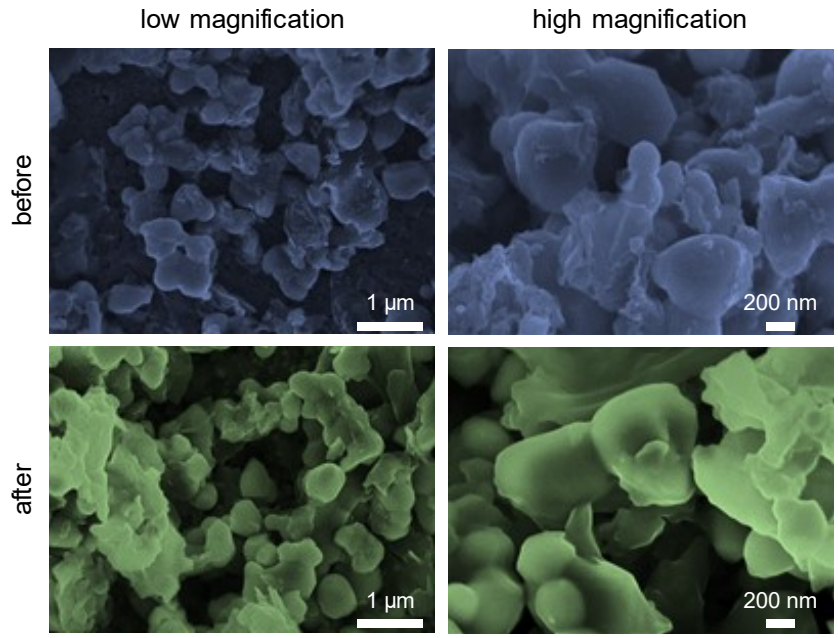

Fig. S14 Electrode material morphology stability. FE-SEM images of the deposited 0.5% Au:LCO/GO (1:3) on Cu foam before and after stability test 15 cycling periods with different magnifications.

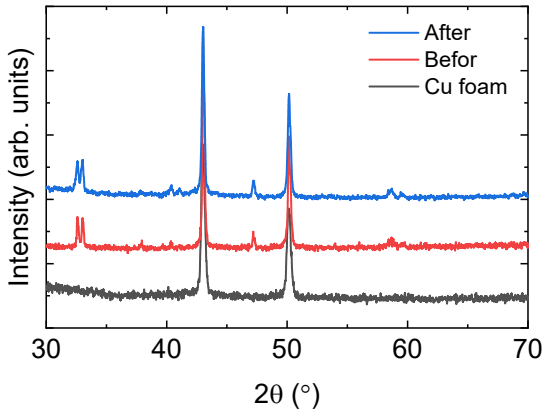

Fig. S15 Electrode material crystal structure stability. XRD patterns of the deposited 0.5% Au:LCO/GO (1:3) on Cu foam before and after 15 cycling periods.

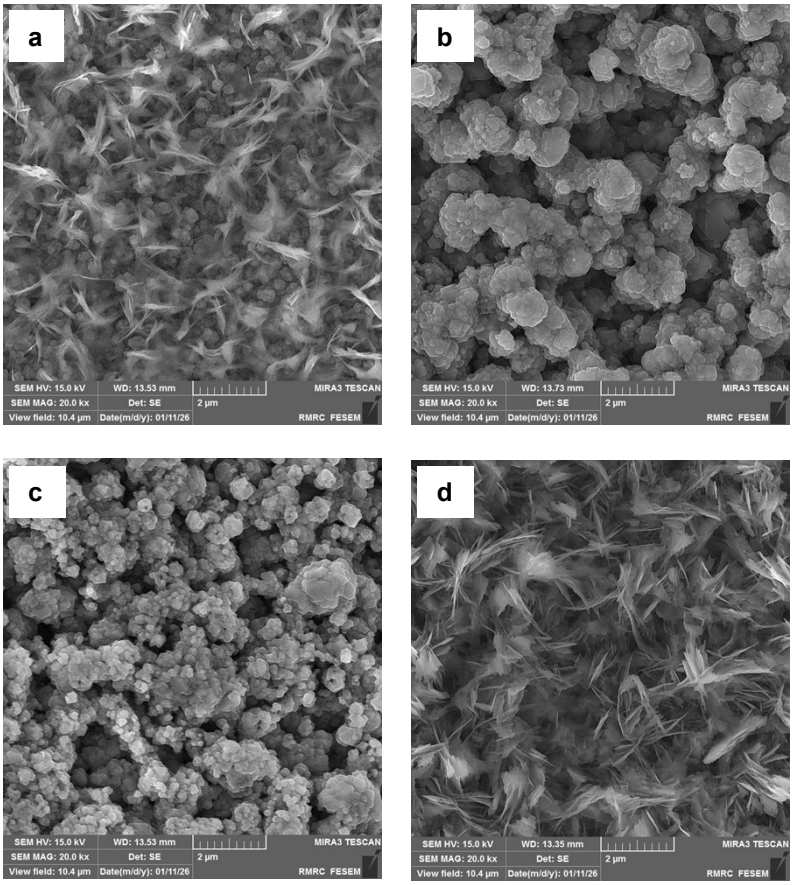

Fig. S16 (a–d) FE-SEM images of the 0.5% Au:LCO/GO (1:3) nanocomposite, 0.5% Au:LCO perovskite, LCO perovskite, and GO after 30 GCD cycles, respectively.

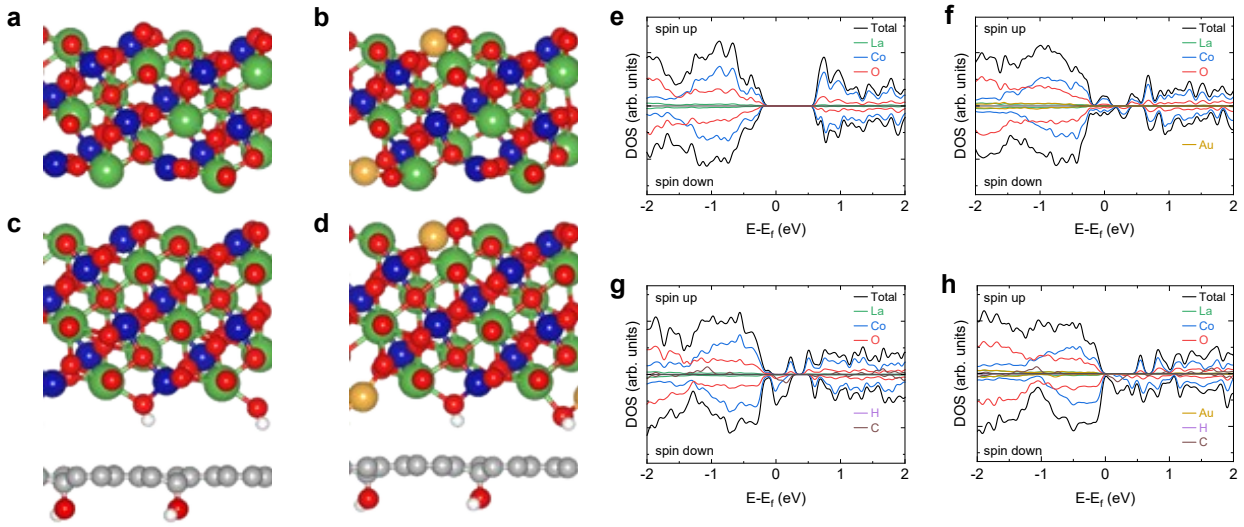

Fig. S17 (a–d) The atomic configurations and **(e–h)** Calculated DOS of LCO, Au:LCO, LCO/GO, and Au:LCO/GO models, respectively. It should be noted that during structural optimization, the OH group of GO spontaneously adsorbs onto the LCO or Au:LCO surfaces. It implies the nanocomposite formation can reduce GO as we observed in the experimental results. Green, blue, red, and orange spheres stand for La, Co, O, and Au atoms, respectively.

Supplementary Tables

Table S1 Reports on electrochemical hydrogen storage properties of ABO_3-based electrodes. RE and N/A stand for the reference electrode and not available, respectively. We have calculated the amount of hydrogen stored W (wt%) for the reported discharge capacity C (mAh g^{-1}) by $W = \frac{3.6C}{F}$ where F is the Faraday constant of 96485.3 C mol^{-1}.[3] Calculated values are indicated by the superscript symbol "$^{\Delta}$".

Year	Material	Electrolyte	RE	C (mAh g^{-1})	W (wt%)	Ref.
2018	$DyFeO_3$	6 M KOH	Ag/AgCl	2100	7.8^{Δ}	[4]
2020	$CdSnO_3$/rGO	6 M KOH	Ag/AgCl	2550	9.5^{Δ}	[5]
2021	$DyFeO_3$/ZnO	2 M KOH	Ag/AgCl	600.1	2.2^{Δ}	[6]
2021	$La_{0.4}Na_{0.6}FeO_3$	12 M KOH	Hg/HgO	356.7	1.3^{Δ}	[7]
2021	$TbFeO_3/Tb_3Fe_5O_{12}$	2 M KOH	Ag/AgCl	490	1.8^{Δ}	[8]
2021	$Sm_{0.5}Sr_{0.5}CoO_{3-\delta}$	6 M KOH	Hg/HgO	182	0.7^{Δ}	[9]
2021	$LaFeO_3/Fe_2O_3$	2 M KOH	Ag/AgCl	790	2.9^{Δ}	[10]
2022	$Dy_3Fe_5O_{12}/DyFeO_3$	2 M KOH	Ag/AgCl	447	1.7^{Δ}	[11]
2022	$LaCoO_3/CoO/La_2O_3$	2 M KOH	Ag/AgCl	1500	5.6^{Δ}	[12]
2023	$LaTiO_3$	N/A	Ag/AgCl	1140	4.1 (4.2^{Δ})	[13]
2023	$GdFeO_3$/g-C_3N_4	2 M KOH	Ag/AgCl	577	2.1^{Δ}	[14]
2023	$LaCrO_3$	6 M KOH	Ag/AgCl	6790	25.3^{Δ}	[15]
	$LaMnO_3$			10500	39.2^{Δ}	
	$LaFeO_3$			13500	50.4^{Δ}	
	$LaCoO_3$			8800	32.8^{Δ}	
	$LaNiO_3$			7000	26.2^{Δ}	

2023	$PrCoO_3/CuO/g\text{-}C_3N_4$	2 M KOH	Ag/AgCl	1200	4.5^{Δ}	[16]
2023	$EuMnO_3/EuMn_2O_5$/MWCNT	2 M KOH	Ag/AgCl	382.5	1.4^{Δ}	[17]
2024	$SrMnO_3/SrCO_3$	2 M KOH	Ag/AgCl	950	3.5^{Δ}	[18]
2024	$LaFe_{0.9}Co_{0.1}O_3$	9 M KOH	Hg/HgO	414	1.5^{Δ}	[19]
2024	$TbCrO_3$/montmorillonite-K10	2 M KOH	Ag/AgCl	734.3	2.7^{Δ}	[20]
2024	$Ni/LaFeO_3$	7 M KOH	Hg/HgO	375.6	1.4^{Δ}	[21]
2025	$FeMnO_3$	3 M KOH	Ag/AgCl	2622	8.9 (9.8^{Δ})	[22]
	$LaCoO_3$			893	3.3	
2025	$LaCo_{1-x}Au_xO_3$/Au	2 M KOH	Ag/AgCl	1264	4.7	This work
	$LaCo_{1-x}Au_xO_3$/Au/GO			2230	8.3	

Table S2 Reports on doped, alloyed, and pristine $LaCoO_3$-based perovskite-type materials used for various applications. NP, rGO, PMMA, PVA, and DFT stand for nanoparticle, reduced graphene oxide, polymethyl methacrylate, polyvinyl alcohol, density functional theory, respectively.

Year	Material	Dopant	Preparation method	Application	Ref.
2002	$LaFe_{0.57}Co_{0.38}Pd_{0.05}O_3$	Pd	alkoxide	catalyst for automotive emissions control	[23]
2007	$La_{1-x}Ce_xCoO_3$	Ce	sol-gel	NO oxidation	[24]
2008	$La_{1-x}Sr_xCoO_{3-\delta}$	Sr	commercially available	magnetic properties in high temperature	[25]
2008	$La_{0.6}Sr_{0.4}Co_{1-y}Fe_yO_{3-\delta}$	Fe	sol-gel	alcohol steam-reforming	[26]
2010	$La_{1-x}Sr_xCoO_3$	Sr	citric acid	NO_x oxidation	[27]
2012	$La_{0.6}Ca_{0.4}CoO_3$	–	sol-gel	oxygen evolution reaction oxygen reduction reaction	[28]
2012	$La_{0.5}Sr_{0.5}CoO_{3-\delta}$	–	pulsed laser deposition	solid oxide fuel cell	[29]
2013	$LaCoO_3$/Au NP	–	PMMA-templating and PVA-protected reduction	CO and toluene oxidation	[30]
2015	$La_{0.6}Ca_{0.4}Mn_xCo_{1-x}O_3$	Mn	modified Pechini process	oxygen evolution reaction	[31]
2016	$La_{1-x}Sr_xCoO_{3-\delta}$	Sr	infiltration and heat treatment	solid oxide fuel cell	[32]
2016	$LaCoO_3$	–	sol-gel	oxygen evolution reaction	[33]
2016	$La_{1-x}Sr_xCoO_{3-\delta}$	Sr	reverse-phase hydrolysis	oxygen evolution reaction	[34]
2017	$LaCo_{3-x}Fe_xO_3$	Fe	sol-gel	oxygen evolution reaction	[35]

2017	$La_{0.5}Sr_{0.5}CoO_{3-\delta}$ $Pr_{0.5}Ba_{0.5}CoO_{3-\delta}$ $SrCoO_{3-\delta}$	–	solid-state reaction	oxygen evolution reaction	36
2017	$LaCoO_3$/Au NP	–	sol-gel	photoelectrochemical water splitting	37
2019	$La_{0.6}Sr_{0.4}CoO_3$	–	pulsed laser deposition	oxygen evolution reaction	38
2019	$La_{0.2}Sr_{0.8}Co_{1-x}Fe_xO_{3-\delta}$	Fe	flame spray synthesis	oxygen evolution reaction	39
2019	$LaCoO_3$	Fe	solid-state reaction	oxygen reduction reaction	40
2019	$LaCo_{1-x}Pt_xO_{3-\delta}$	Pt	sol-gel	oxygen evolution reaction hydrogen evolution reaction	41
2019	$La_{1-x}Sr_xCoO_{3-\delta}$	Sr	sol-gel	oxygen evolution reaction	42
2020	$La_{1-x}Sr_xCoO_{3-\delta}$	Sr	pulsed laser deposition	oxygen evolution reaction	43
2020	$La_{0.6}Sr_{0.4}CoO_{3-\delta}$	–	Pechini process	solid oxide fuel cell	44
2020	$LaCo_{0.8}X_{0.2}O_3$	Al, Ni, Zn	citrate route	CO oxidation NO oxidation N_2O decomposition	45
2020	$LaCoO_3$	Ce	sol-gel	zinc-air battery	46
2020	$LaCo_{1-x}Ru_xO_{3-\delta}$	Ru	modified citrate sol-gel (Pechini process)	zinc-air battery	47
2021	$LaCoO_3$	–	pulsed laser deposition	transport and magnetic properties	48
2021	$La_{1-x}Ce_xCoO$	Ce	hydrothermal	hydrogen evolution reaction oxygen evolution reaction	49
2021	$LaCoO_3$	–	solid-state	insight into the structure of	50

			reaction	Ruddlesden–Popper phases	
2021	$La_{1-x}Ag_xCoO_3$	Ag	sodium EDTA–citric acid complexation	catalytic oxidation of soot	[51]
2021	$La_{0.6}Sr_{0.4}Co_{0.2}Fe_{0.8}O_{3-\delta}$	–	tape casting–lamination	solid oxide electrochemical cells	[52]
2021	$LaCoO_3$	Fe, Cr, Mn, Sc, Al, In	sol-gel	oxygen evolution reaction	[53]
2021	$LaCoO_3$	Ni, Mn	hydrothermal	oxygen evolution reaction oxygen reduction reaction	[54]
2021	$La_{0.8}Sr_{0.2}Mn_{0.5}Co_{0.5}O_3/RuO_x$	–	sol-gel	zinc-air battery	[55]
2021	$LaCoO_{3-\delta}$/Ag NP	–	solid-state reaction	oxygen reduction reaction	[56]
2022	$(La_{0.8}Sr_{0.2})_{0.9}Co_{0.1}Fe_{0.8}Ru_{0.1}O_{3-\delta}$	Ru	solid-state reaction	oxygen evolution reaction	[57]
2022	$La_{0.9}Ce_{0.05}K_{0.05}CoO_3$	Ce, K	sol-gel	soot combustion	[58]
2022	$La_{1-x}Sr_xCoO_3$	Sr	sol-gel	oxygen evolution reaction	[59]
2022	$LaCoO_3$	–	sol-gel	propane oxidation	[60]
2022	$La_{0.6}Sr_{0.4}CoO_{3-\delta}$	–	pulsed laser deposition	oxygen evolution reaction	[61]
2022	$La_{1-x}Sr_xCoO_{3-\delta}$	Sr	pulsed laser deposition	oxygen evolution reaction	[62]
2023	$LaCoO_3$	–	solid-state reaction	spin-triplet exciton condensations at ultrahigh magnetic fields	[63]
2023	$La_{0.5}Ce_{0.5}CoO_{3-\delta}$	–	self-propagation high temperature synthesis	toluene oxidation in the plasma-catalytic system	[64]
2023	$LaCoO_3$	–	pulsed laser	magnetic properties	[65]

			deposition		
2023	$LaCoO_3$	–	sol-gel	H_2S oxidation	[66]
2023	$La_{0.5}Sr_{0.5}CoO_{3-\delta}$	–	high-pressure-oxygen sputtering	electronic transport and thermal conductivity	[67]
2023	$LaCoO_3$	–	sol-gel	oxygen evolution reaction	[68]
2023	$LaCoO_3$	Sr, Mn	Citrate route	catalytic benzene combustion	[69]
2023	$LaCo_{1-x}Zn_xO_3$	Zn	sol-gel	oxygen evolution reaction	[70]
2023	$LaCoO_3$	Ba	self-propagating high-temperature synthesis	zinc-air battery	[71]
2023	$LaMn_xCo_{1-x}O_3$	Mn	sol-gel	nitrate reduction	[72]
2023	$LaCoO_3$	F	sol-gel	oxygen evolution reaction oxygen reduction reaction	[73]
2024	$LaCoO_3$	–	pulsed laser deposition	axon-like active signal transmission	[74]
2024	$LaCoO_3$	–	sol-gel hydrothermal	supercapacitor	[75]
2024	$BaGd_{0.3}La_{0.7}Co_2O_{6-\delta}$	–	solid-state reaction	protonic electrical conductivity	[76]
2024	$LaCoO_3$	–	pulsed laser deposition	true random number generation	[77]
2024	$LaCoO_3$	–	sol-gel autocombustion	CO oxidation	[78]
2024	$LaCoO_3$	Ca	hydrothermal	oxygen evolution reaction	[79]
2024	$LaCoO_3$	Mn, Cr, Fe, Ti	DFT calculations	oxygen evolution reaction oxygen reduction reaction	[80]
2024	$La_{1-x}Sr_xCoO_{3-\delta}$	Sr	solid-state	electric transport	[81]

			reaction		
2024	$LaCo_{0.9}O_{3-\delta}$	–	sol-gel	CO oxidation	[82]
2024	$La_{0.6}Sr_{0.4}CoO_3$	–	sol-gel	oxygen evolution reaction	[83]
2025	$LaCoO_3$	–	sol-gel	atrazine degradation in water	[84]
2025	$LaCoO_3$ $LaCo_{1-x}Au_xO_3$/Au $LaCo_{1-x}Au_xO_3$/Au/GO	Au	sol-gel	electrochemical hydrogen storage	This work

Table S3 Reports on $LaCoO_3$-based perovskite-type composite electrodes used for electrochemical applications. AB, MWCNT, and rGO stand for acetylene black, multi-walled carbon nanotubes, reduced graphene oxide, respectively.

Year	Material	Preparation method	Application	Ref.
2016	$LaCoO_3$/rGO	sol-gel	lithium-oxygen battery	[85]
2017	$LaCoO_3$/N:rGO	sol-gel	oxygen evolution reaction oxygen reduction reaction	[86]
2021	$La_{0.5}Ca_{0.5}CoO_{3-\delta}$/rGO	modified citrate	zinc-air battery	[87]
2022	$LaCoO_3$/rGO	solvothermal	supercapacitor	[88]
2022	$LaCoO_3$/rGO	precipitation-deposition	water–gas shift reaction	[89]
2022	$LaCoO_3$/rGO	sol-gel	supercapacitor	[90]
2023	$LaCoO_3$/rGO	sol-gel	oxygen evolution reaction oxygen reduction reaction	[91]
2024	$LaCoO_3$/AB $LaCoO_3$/MWCNT $LaCoO_3$/rGO	sol-gel	oxygen evolution reaction	[92]
2025	$LaCoO_3$ $LaCo_{1-x}Au_xO_3$/Au $LaCo_{1-x}Au_xO_3$/Au/GO	sol-gel	electrochemical hydrogen storage	This work

Table S4 BET data of the LCO and 0.5% Au:LCO samples.

Sample	BET surface area	Total volume	Average diameter

	(m^2 g^{-1})	(cm^3 g^{-1})	(nm)
LCO	22.3	0.040	6.9
0.5% Au:LCO	67.2	0.089	5.3

Table S5 Peak positions of the XPS fitted Co 2*p* spectra of LCO and 0.5% Au:LCO. FWHMs are written inside the parentheses.

LCO		**0.5% Au:LCO**	
Co 2*p* multiplets (eV)	Co 2*p* satellites (eV)	Co 2*p* multiplets (eV)	Co 2*p* satellites (eV)
778.96 (1.94)	785.98 (3.51)	779.09 (1.75)	786.12 (3.94)
780.18 (2.05)	789.91 (4.12)	780.03 (2.19)	789.76 (3.25)
781.76 (2.94)	800.97 (5.15)	781.72 (2.83)	801.11 (4.51)
783.88 (2.37)	805.55 (5.99)	784.02 (2.16)	804.96 (5.99)
793.95 (2.20)		794.08 (2.16)	
795.17 (2.15)		795.24 (2.42)	
796.74 (2.4)		796.71 (2.71)	
798.87 (1.90)		799.01 (1.99)	

Table S6 Lattice parameters of optimized LCO unit cell and three possible Au-substituted configurations by r^2SCAN.

System	Magnetic moment (μB)	Configuration	a (Å)	b (Å)	c (Å)
LCO	0.00	$La_6Co_6O_{18}$	5.428	5.441	13.039
Au_{La}	4.00	$Au_1La_5Co_6O_{18}$	5.359	5.356	13.308
Au_{Co}	0.00	$Au_1La_6Co_5O_{18}$	5.341	5.513	13.638
Au_O	3.00	$Au_1La_6Co_6O_{17}$	5.449	5.563	13.710

Table S7 Calculated $^{\Delta H_{cal}}$ of possible secondary phases by r^{2}SCAN.

Materials	Space group	ΔH_{cal} (eV)	Materials	Space group	ΔH_{cal} (eV)
Co_3O_4	$Fd\bar{3}m$	-9.42	La_2CoO_4	$I4/mmm$	-20.84
CoO_2	$R\bar{3}m$	-2.91	$La_4(CoO_3)_3$	$Pnma$	-43.88
CoO	$F\bar{4}3m$	-2.20	$La_4Co_3O_{10}$	$P2_1/c$	-47.05
La_2O_3	$P\bar{3}m1$	-18.78	$La_2Co_2O_5$	$Pnma$	-22.95
LaO_2	$P2_1/m$	-8.77	$La_3Co_3O_8$	$P2_1$	-36.04
LaO_3	$P6_1/m$	-7.08	Au_2O_3	$Fdd2$	-0.84
$LaCoO_3$	$R\bar{3}c$	-13.02			

Table S8 Bader charge analysis for pristine and Au-doped LCO for Au_{La}, Au_{Co}, and Au_{Co} substitutions.

No.	Pristine			Au_{La}			Au_{Co}			Au_{O}		
	Atom	V.E.	Q.	Atom	V.E.	Q.	Atom	V.E.	Q.	Atom	V.E.	Q.
1	La	8.85	+2.15	La	8.85	+2.15	La	8.86	+2.14	**La**	**8.91**	**+2.09**
2	La	8.85	+2.15	La	8.85	+2.15	La	8.84	+2.16	La	8.84	+2.16
3	La	8.85	+2.15	La	8.82	+2.18	La	8.85	+2.15	La	8.86	+2.14
4	La	8.85	+2.15	**Au**	**9.93**	**+1.07**	La	8.85	+2.15	La	8.87	+2.13
5	La	8.85	+2.15	La	8.85	+2.15	La	8.86	+2.14	**La**	**8.98**	**+2.02**
6	La	8.85	+2.15	Co	7.58	+1.42	La	8.85	+2.15	La	8.84	+2.16
7	Co	7.58	+1.42	Co	7.60	+1.40	Co	7.58	+1.42	Co	7.59	+1.41
8	Co	7.58	+1.42	**Co**	**7.52**	**+1.48**	Co	7.58	+1.42	**Co**	**7.84**	**+1.16**
9	Co	7.58	+1.42	Co	7.58	+1.42	**Au**	**9.96**	**+1.04**	**Co**	**7.84**	**+1.16**
10	Co	7.58	+1.42	Co	7.59	+1.41	Co	7.57	+1.43	Co	7.58	+1.42
11	Co	7.58	+1.42	Co	7.57	+1.43	Co	7.58	+1.42	Co	7.60	+1.40
12	Co	7.58	+1.42	La	8.85	+2.15	Co	7.58	+1.42	Co	7.61	+1.39
13	O	7.19	-1.19	O	7.19	-1.19	O	7.20	-1.20	O	7.18	-1.18
14	O	7.19	-1.19	O	7.18	-1.18	O	7.19	-1.19	O	7.21	-1.21
15	O	7.20	-1.20	O	7.19	-1.19	O	7.21	-1.21	O	7.22	-1.22
16	O	7.19	-1.19	O	7.16	-1.16	O	7.18	-1.18	O	7.23	-1.23
17	O	7.20	-1.20	**O**	**7.03**	**-1.03**	**O**	**7.08**	**-1.08**	O	7.17	-1.17
18	O	7.19	-1.19	O	7.14	-1.14	**O**	**7.07**	**-1.07**	O	7.17	-1.17
19	O	7.19	-1.19	**O**	**7.03**	**-1.03**	**O**	**7.07**	**-1.07**	O	7.16	-1.16
20	O	7.20	-1.20	**O**	**7.04**	**-1.04**	**O**	**7.08**	**-1.08**	**Au**	**11.28**	**-0.28**
21	O	7.19	-1.19	**O**	**6.98**	**-0.98**	O	7.18	-1.18	O	7.19	-1.19
22	O	7.19	-1.19	**O**	**7.02**	**-1.02**	O	7.21	-1.21	O	7.23	-1.23
23	O	7.19	-1.19	O	7.12	-1.12	O	7.19	-1.19	O	7.22	-1.22
24	O	7.20	-1.20	O	7.17	-1.17	O	7.21	-1.21	O	7.21	-1.21
25	O	7.19	-1.19	O	7.17	-1.17	O	7.19	-1.19	O	7.19	-1.19
26	O	7.20	-1.20	O	7.21	-1.21	O	7.21	-1.21	O	7.20	-1.20
27	O	7.19	-1.19	O	7.19	-1.19	O	7.19	-1.19	O	7.19	-1.19
28	O	7.20	-1.20	O	7.22	-1.22	O	7.21	-1.21	O	7.19	-1.19
29	O	7.19	-1.19	O	7.19	-1.19	O	7.19	-1.19	O	7.19	-1.19
30	O	7.19	-1.19	O	7.19	-1.19	O	7.19	-1.19	O	7.20	-1.20

Number of valance electron (V.E.) and Charge (Q.) in unit C

Table S9 The amount of H_2 evolved during the GCD processes corresponding to the conditions illustrated in Fig. 6b.

Zone in Fig. 6b	Amount of H_2 (ppm)
Zone A	Not detected
Zone B	Not detected
Zone C	Not detected
Point D	6
Point E	26
Zone F	54

Table S10 The values of fitted elements for the utilized equivalent circuits, $R_s + [R_{ct,1}||CPE_1]$, $R_s + [R_{ct,1}||CPE_1] + [R_{ct,2}||CPE_2]$, and $R_s + [R_{ct,1}||CPE_1]||[R_{ct,3}||CPE_3] + [R_{ct,2}||CPE_2]$.

GO		LCO		0.5% Au:LCO		0.5% Au:LCO/GO (1:3)	
Elements	**Values**	**Elements**	**Values**	**Elements**	**Values**	**Elements**	**Values**
R_s (Ω)	1.2	R_s (Ω)	0.13	R_s (Ω)	0.22	R_s (Ω)	0.71
$R_{ct,1}$ (Ω)	131	$R_{ct,1}$ (Ω)	79.0	$R_{ct,1}$ (Ω)	53.5	$R_{ct,1}$ (Ω)	0.02
$P1$ (F)	4.8×10^{-3}	$R_{ct,2}$ (Ω)	45.8	$R_{ct,2}$ (Ω)	92.0	$R_{ct,2}$ (Ω)	277.8
$n1$	0.84	P_1 (F)	2.7×10^{-4}	P_1 (F)	3.0×10^{-4}	$R_{ct,3}$ (Ω)	21.7
		n_1	0.87	n_1	0.77	P_1 (F)	7.0×10^{-4}
		P_2 (F)	4.3×10^{-3}	P_2 (F)	9.3×10^{-3}	n_1	0.50
		n_2	0.87	n_2	0.61	P_2 (F)	4.4×10^{-2}
		W (Ω)	53.2	W (Ω)	41.0	n_2	0.86
						P_3 (F)	4.5×10^{-3}
						n_3	0.78
						W (Ω)	0.1

Supplementary References

1. T. Ofoegbuna, P. Darapaneni, S. Sahu, C. Plaisance and J. A. Dorman, *Nanoscale*, 2019, **11**, 14303-14311.

2. H. Sadabadi, S. R. Allahkaram, A. Kordijazi, O. Akbarzadeh and P. K. Rohatgi, *Eng. Rep.*, 2021, **3**, e12335.

3. X. L. Xu, Y. Dong, Q. W. Hu, N. Si and C. W. Zhang, *Energ Fuel*, 2024, **38**, 7579-7613.

4. A. Salehabadi, M. Salavati-Niasari, T. Gholami and A. Khoobi, *Int. J Hydrogen Energ.*, 2018, **43**, 9713-9721.

5. M. Masjedi-Arani, M. Ghiyasiyan-Arani, O. Amiri and M. Salavati-Niasari, *Ultrason. Sonochem.*, 2020, **61**, 104840.

6. M. Baladi, M. Valian, M. Ghiyasiyan-Arani and M. Salavati-Niasari, *Int. J. Hydrogen. Energ.*, 2021, **46**, 21026-21039.

7. K. Ren, Z. Duan, Y. Li, L. Zhang and S. Han, *J. Electrochem. Soc.*, 2021, **168**, 043501.

8. P. Mehdizadeh, M. Masjedi-Arani, O. Amiri and M. Salavati-Niasari, *Fuel*, 2021, **304**, 121412.

9. A. Bhardwaj, H. Bae, I.-H. Kim, L. Mathur, J.-Y. Park and S.-J. Song, *J. Electrochem. Soc.*, 2021, **168**, 070540.

10. P. Mehdizadeh, M. Masjedi-Arani and M. Salavati-Niasari, *Int. J. Hydrogen. Energ.*, 2021, **46**, 17253-17266.

11. S. Alinavaz, M. Ghiyasiyan-Arani and M. Salavati-Niasari, *Fuel*, 2022, **324**, 124600.

12. P. Mehdizadeh, M. Masjedi-Arani, O. Amiri, A. Al-Nayili and M. Salavati-Niasari, *Fuel*, 2022, **311**, 122544.

13. M. Valian, A. Salehabadi and M. Salavati-Niasari, *Int. J. Hydrogen. Energ.*, 2023, **48**, 4762-4772.

14. R. Mohassel, M. Shabani-Nooshabadi and M. Salavati-Niasari, *Int. J. Hydrogen. Energ.*, 2023, **48**, 6586-6596.

15. M. Ostadebrahim and O. Moradlou, *J. Energy Storage*, 2023, **72**, 108284.

16. M. Baladi, E. A. Dawi and M. Salavati-Niasari, *J. Energy Storage*, 2023, **63**, 106999.

17. Z. Heydariyan, R. Monsef, E. A. Dawi and M. Salavati-Niasari, *Fuel*, 2023, **351**, 128885.

18. S. A. Ehsanizadeh, A. S. Abbas, F. S. Razavi, E. A. Dawi, A. M. M. Ibrahim and M. Salavati-Niasari, *Int. J. Hydrogen. Energ.*, 2024, **60**, 392-401.

19. S. Sun, G. Zhang, Z. Yang, L. Bai, Y. Li, Z. Liu, J. Xu, R. Guo and Y. Zhang, *Ceram. Int.*, 2024, **50**, 42176-42187.

20. Z. Heydariyan, M. Salavati-Niasari and R. Monsef, *Fuel*, 2024, **372**, 132177.

21. J. Xu, G. Zhang, X. Zhao, F. Hu and D. Ke, *Nano Select*, 2024, **5**, 2300091.

22. S. Abdollah Lachini, A. Eslami and Q. Chu, *J. Alloy Compd.*, 2025, **1010**, 177486.

23. Y. Nishihata, J. Mizuki, T. Akao, H. Tanaka, M. Uenishi, M. Kimura, T. Okamoto and N. Hamada, *Nature*, 2002, **418**, 164-167.

24. Y. Wen, C. Zhang, H. He, Y. Yu and Y. Teraoka, *Catal. Today*, 2007, **126**, 400-405.

25. D. Baskar and S. B. Adler, *Chem. Mater.*, 2008, **20**, 2624-2628.

26. M. M. Natile, F. Poletto, A. Galenda, A. Glisenti, T. Montini, L. De Rogatis and P. Fornasiero, *Chem. Mater.*, 2008, **20**, 2314-2327.

27. C. H. Kim, G. Qi, K. Dahlberg and W. Li, *Science*, 2010, **327**, 1624-1627.

28. S. Malkhandi, B. Yang, A. K. Manohar, A. Manivannan, G. K. Prakash and S. R. Narayanan, *J. Phys. Chem. Lett.*, 2012, **3**, 967-972.

29. Y. M. Kim, J. He, M. D. Biegalski, H. Ambaye, V. Lauter, H. M. Christen, S. T. Pantelides, S. J. Pennycook, S. V. Kalinin and A. Y. Borisevich, *Nat. Mater.*, 2012, **11**, 888-894.

30. X. W. Li, H. X. Dai, J. G. Deng, Y. X. Liu, S. H. Xie, Z. X. Zhao, Y. Wang, G. S. Guo and H. Arandiyan, *Chem. Eng. J.*, 2013, **228**, 965-975.

31. S. Malkhandi, P. Trinh, A. K. Manohar, A. Manivannan, M. Balasubramanian, G. K. S. Prakash and S. R. Narayanan, *J. Phys. Chem. C.*, 2015, **119**, 8004-8013.

32. K. Tamm, P. Möller, G. Nurk and E. Lust, *J. Electrochem. Soc.*, 2016, **163**, F586-F592.

33. S. Zhou, X. Miao, X. Zhao, C. Ma, Y. Qiu, Z. Hu, J. Zhao, L. Shi and J. Zeng, *Nat. Commun.*, 2016, **7**, 11510.

34. J. T. Mefford, X. Rong, A. M. Abakumov, W. G. Hardin, S. Dai, A. M. Kolpak, K. P. Johnston and K. J. Stevenson, *Nat. Commun.*, 2016, **7**, 11053.

35. Y. Duan, S. N. Sun, S. B. Xi, X. Ren, Y. Zhou, G. L. Zhang, H. T. Yang, Y. H. Du and Z. C. J. Xu, *Chem. Mater.*, 2017, **29**, 10534-10541.

36. A. Grimaud, O. Diaz-Morales, B. Han, W. T. Hong, Y. L. Lee, L. Giordano, K. A. Stoerzinger, M. T. M. Koper and Y. Shao-Horn, *Nat. Chem.*, 2017, **9**, 457-465.

37. B. T. Zhang, J. Liu, S. Z. Yue, Y. G. Teng, Z. J. Wang, X. B. Li, S. C. Qu and Z. G. Wang, *Appl. Catal. B*, 2017, **219**, 432-438.

38. M. L. Weber, C. Baeumer, D. N. Mueller, L. Jin, C. L. Jia, D. S. Bick, R. Waser, R. Dittmann, I. Valov and F. Gunkel, *Chem. Mater.*, 2019, **31**, 2337-2346.

39. B. J. Kim, E. Fabbri, D. F. Abbott, X. Cheng, A. H. Clark, M. Nachtegaal, M. Borlaf, I. E. Castelli, T. Graule and T. J. Schmidt, *J. Am. Chem. Soc.*, 2019, **141**, 5231-5240.

40. M. Wang, B. Han, J. Deng, Y. Jiang, M. Zhou, M. Lucero, Y. Wang, Y. Chen, Z. Yang, A. T. N'Diaye, Q. Wang, Z. J. Xu and Z. Feng, *ACS Appl. Mater. Interfaces*, 2019, **11**, 5682-5686.

41. C. Wang, L. Zeng, W. Guo, C. Gong and J. Yang, *Rsc Adv*, 2019, **9**, 35646-35654.

42. Y. Lu, A. J. Ma, Y. F. Yu, R. Tan, C. W. Liu, P. Zhang, D. Liu and J. Z. Gui, *ACS Sustain. Chem. Eng.*, 2019, **7**, 2906-2910.

43. A. Boucly, E. Fabbri, L. Artiglia, X. Cheng, D. Pergolesi, M. Ammann and T. J. Schmidt, *Chem. Mater.*, 2020, **32**, 5256-5263.

44. Y. P. Ivanov, M. Kubicek, M. Siebenhofer, A. Viernstein, H. Hutter, J. Fleig, A. Chuvilin and Z. Zhang, *Commun. Mater.*, 2020, **1**, 25.

45. J. Simbock, M. Ghiasi, S. Schonebaum, U. Simon, F. M. F. de Groot and R. Palkovits, *Nat. Commun.*, 2020, **11**, 652.

46. J. M. Qian, T. T. Wang, Z. M. Zhang, Y. G. Liu, J. F. Li and D. Q. Gao, *Nano Energy*, 2020, **74**, 104948.

47. S. G. Chandrappa, P. Moni, D. Chen, G. Karkera, K. R. Prakasha, R. A. Caruso and A. S. Prakash, *J. Mater. Chem. A*, 2020, **8**, 20612-20620.

48. M. Meng, Y. Sun, Y. Li, Q. An, Z. Wang, Z. Lin, F. Yang, X. Zhu, P. Gao and J. Guo, *Nat. Commun.*, 2021, **12**, 2447.

49. D. Ji, C. Liu, Y. Yao, L. Luo, W. Wang and Z. Chen, *Nanoscale*, 2021, **13**, 9952-9959.

50. Y. Hong, P. Byeon, J. Bak, Y. Heo, H. S. Kim, H. B. Bae and S. Y. Chung, *Nat. Commun.*, 2021, **12**, 5527.

51. L. J. He, Y. Zhang, Y. C. Zang, C. X. Liu, W. C. Wang, R. Han, N. Ji, S. T. Zhang and Q. L. Liu, *Acs Catal.*, 2021, **11**, 14224-14236.

52. J. Lee, M. Kim, Y. Lee and J. H. Joo, *Chem. Mater.*, 2021, **33**, 6290-6298.

53. T. G. Yun, Y. Heo, H. Bin Bae and S. Y. Chung, *Nat. Commun.*, 2021, **12**, 824.

54. J. Sun, L. Du, B. Y. Sun, G. K. Han, Y. L. Ma, J. J. Wang, H. Huo, P. J. Zuo, C. Y. Du and G. P. Yin, *J. Energy Chem.*, 2021, **54**, 217-224.

55. Y. Dai, J. Yu, Z. Zhang, S. Zhai, C. Cheng, S. Zhao, P. Tan, Z. Shao and M. Ni, *ACS Appl. Mater. Interfaces*, 2021, **13**, 61098-61106.

56. Y. Liang, D. D. Ye, N. Han, P. Liang, J. Q. Wang, G. J. Yang, C. K. Zhang, X. He, M. Chen and C. Zhang, *Electrochim. Acta*, 2021, **391**, 138908.

57. Y. Liang, Y. Cui, Y. Chao, N. Han, J. Sunarso, P. Liang, X. He, C. Zhang and S. M. Liu, *Nano Res.*, 2022, **15**, 6977-6986.

58. D. Yu, L. Y. Wang, C. L. Zhang, C. Peng, X. H. Yu, X. Q. Fan, B. Liu, K. X. Li, Z. G. Li, Y. C. Wei, J. Liu and Z. Zhao, *Acs Catal.*, 2022, **12**, 15056-15075.

59. Z. Shen, M. Qu, J. Shi, F. E. Oropeza, V. A. de la Peña O'Shea, G. Gorni, C. M. Tian, J. P. Hofmann, J. Cheng, J. Li and K. H. L. Zhang, *J. Energy. Chem.*, 2022, **65**, 637-645.

60. C. Feng, Q. Q. Gao, G. Y. Xiong, Y. F. Chen, Y. Pan, Z. Y. Fei, Y. P. Li, Y. K. Lu, C. G. Liu and Y. Q. Liu, *Appl. Catal. B*, 2022, **304**, 121005.

61. M. L. Weber, G. Lole, A. Kormanyos, A. Schwiers, L. Heymann, F. D. Speck, T. Meyer, R. Dittmann, S. Cherevko, C. Jooss, C. Baeumer and F. Gunkel, *J. Am. Chem. Soc.*, 2022, **144**, 17966-17979.

62. Y. D. Ren, J. Oyama, T. Uchiyama, Y. Orikasa, T. Watanabe, K. Yamamoto, T. Takami, Y. Nishiki, S. Mitsushima and Y. Uchimoto, *Acs Appl. Energ. Mater.*, 2022, **5**, 4108-4116.

63. A. Ikeda, Y. H. Matsuda, K. Sato, Y. Ishii, H. Sawabe, D. Nakamura, S. Takeyama and J. Nasu, *Nat. Commun.*, 2023, **14**, 1744.

64. B. Zhu, Q.-W. Li, Y.-C. Li, Y.-Q. Xia, J.-L. Liu, A. M. Zhou and X.-M. Zhang, *Chem. Eng. J.*, 2023, **469**, 143897.

65. D. Li, H. Wang, K. Li, B. Zhu, K. Jiang, D. Backes, L. S. I. Veiga, J. Shi, P. Roy, M. Xiao, A. Chen, Q. Jia, T. L. Lee, S. S. Dhesi, D. O. Scanlon, J. L. MacManus-Driscoll, P. A. van Aken, K. H. L. Zhang and W. Li, *Nat. Commun.*, 2023, **14**, 3638.

66. X. H. Zheng, B. Li, L. J. Shen, Y. N. Cao, Y. Y. Zhan, S. T. Zheng, S. P. Wang and L. L. Jiang, *Appl. Catal. B*, 2023, **329**, 122526.

67. Y. Zhang, W. M. Postiglione, R. Xie, C. Zhang, H. Zhou, V. Chaturvedi, K. Heltemes, H. Zhou, T. Feng, C. Leighton and X. Wang, *Nat. Commun.*, 2023, **14**, 2626.

68. M. Y. Wang, K. C. Chukwu, B. A. Muhich, W. S. Samarakoon, Z. Z. He, M. Lucero, C. W. Chang, A. L. Chang, D. Q. Yang, S. Kaur, A. T. N'Diaye, G. E. Sterbinsky, Y. G. Du, L. Fei, L. Arnadóttir and Z. X. Feng, *Electrochim. Acta*, 2023, **466**, 143034.

69. Z. Shi, F. Dong, Z. C. Tang and X. Y. Dong, *Chem. Eng. J.*, 2023, **473**, 145476.

70. F. Hadji, M. Omari and M. Mebarki, *Ceram. Int.*, 2023, **49**, 25405-25413.

71. H. Zhou, W. Zhao, Z. M. Lu, S. C. He, B. Yin, Y. F. Zheng, L. Ge and H. Chen, *Electrochim. Acta*, 2023, **462**, 142757.

72. W. Z. Zhang, F. K. Li, W. Zhang, Y. Wang, S. Liu, X. P. Mo and K. X. Li, *Sep. Purif. Technol.*, 2023, **317**, 123775.

73. J. Ran, L. Wang, M. Si, X. Liang and D. Gao, *Small*, 2023, **19**, e2206367.

74. T. D. Brown, A. Zhang, F. U. Nitta, E. D. Grant, J. L. Chong, J. Zhu, S. Radhakrishnan, M. Islam, E. J. Fuller, A. A. Talin, P. J. Shamberger, E. Pop, R. S. Williams and S. Kumar, *Nature*, 2024, **633**, 804-810.

75. K. Moorthi, B. Sivakumar, B. Chokkiah, H. Valdes and S. Mohan, *ACS Appl. Nano Mater.*, 2024, **7**, 18511-18522.

76. T. Miruszewski, R. Strandbakke, K. Dzierzgowski, I. Szpunar, A. Mielewczyk-Gryn, S. Wachowski and M. Gazda, *J. Mater. Chem. A*, 2024, **12**, 13488-13497.

77. K. S. Woo, A. Zhang, A. Arabelo, T. D. Brown, M. Park, A. A. Talin, E. J. Fuller, R. S. Bisht, X. Qian, R. Arroyave, S. Ramanathan, L. Thomas, R. S. Williams and S. Kumar, *Nat. Commun.*, 2024, **15**, 4656.

78. A. Abouserie, D. Rohrens, D. Formenti, X. C. Wu, L. Patterer, F. Ott, G. Dalfollo, J. M. Schneider, R. Palkovits and U. Simon, *J. Phys. Chem. C*, 2024, **128**, 3281-3294.

79. F. Bai, J. Schulwitz, T. Priamushko, U. Hagemann, A. Kostka, M. Heidelmann, S. Cherevko, M. Muhler and T. Li, *J. Catal.*, 2024, **438**, 115697.

80. H. P. Chen, H. A. Xie, C. Yang, J. S. Pang, N. Q. Zhao, C. N. He and E. Z. Liu, *Electrochim. Acta*, 2024, **491**, 144339.

81. S. Biswas, N. Naushad, K. S and V. B. Kamble, *ACS Mater. Au*, 2024, **4**, 308-323.

82. M. Kim, J. Cho, K. Tae Park, C. Houn Rhee, H. Woong Park and J. Chul Jung, *J. Ind. Eng. Chem.*, 2024, **139**, 250-257.

83. H. Yu, N. Liedienov, I. Zatovsky, D. Butenko, I. Fesych, W. Xu, C. Song, Q. Li, B. Liu, A. Pashchenko and G. Levchenko, *ACS Appl. Mater. Interfaces*, 2024, **16**, 3605-3620.

84. S. Afzal, A. Mehmood, L. Jin, K. Pan, M. Ahmad, M. Javid, M. Ikram, M. Zhang and L. Liu, *Sep. Purif. Technol.*, 2025, **354**, 128823.

85. M. Lu, C. Xu, Y. Zhan and J. Y. Lee, *Chem. Asian. J.*, 2016, **11**, 1210-1217.

86. K. Liu, J. Li, Q. F. Wang, X. P. Wang, D. Qian, J. B. Jiang, J. H. Li and Z. H. Chen, *J. Alloy Compd*, 2017, **725**, 260-269.

87. S. X. Zhuang, Z. H. Wang, J. Y. He, D. L. Jia, Q. B. Wang, M. Lu and F. Y. Tu, *Sustain. Mater. Techno.*, 2021, **29**, e00282.

88. A. K. Vats, A. Kumar, P. Rajput and A. Kumar, *J. Mater. Sci.: Mater. Electron.*, 2022, **33**, 2590-2606.

89. T. R. Mignoli, T. L. R. Hewer, R. M. B. Alves and M. Schmal, *Appl. Catal. A*, 2022, **635**, 118553.

90. M. N. Lu, H. Li, S. J. M. Li, F. C. Yang, Y. Cao and W. F. Qiu, *Sustain. Energy Fuels*, 2022, **6**, 3453-3464.

91. J. Ahmed, T. Ahamad, N. Alhokbany, M. A. Majeed Khan, P. Arunachalam, M. S. Amer, R. M. Alotaibi and S. M. Alshehri, *J. Ind. Eng. Chem.*, 2023, **121**, 100-106.

92. A. K. Rana and A. A. Hussain, *J. Mater. Sci.*, 2024, **59**, 17128-17144.